iScience

Article

Rapid and sensitive antimicrobial susceptibility testing of biofilm-forming bacteria using scalable paper-based organic transistors

Graphical abstract

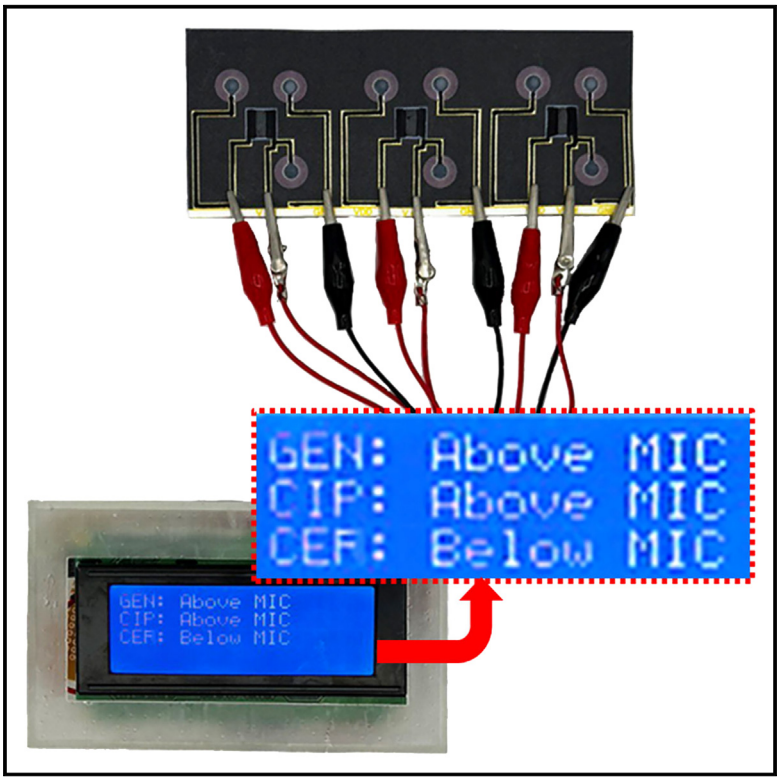

Authors

Zahra Rafiee, Maryam Rezaie, Seokheun Choi

Correspondence

sechoi@binghamton.edu

In brief

Analytical chemistry; Bioelectronics; Electronic materials

Highlights

- A paper-based organic field-effect transistor platform is developed for rapid AST
- It offers a clinically translatable solution for monitoring biofilm treatment efficacy
- It tracks protons generated by pathogenic biofilms
- It delivers rapid, on-site diagnostics with minimal resource demands

Rafiee et al., 2025, iScience *28*, 112312
April 18, 2025
https://doi.org/10.1016/j.isci.2025.112312

CellPress

iScience

CellPress
OPEN ACCESS

Article

Rapid and sensitive antimicrobial susceptibility testing of biofilm-forming bacteria using scalable paper-based organic transistors

Zahra Rafiee,[1] Maryam Rezaie,[1] and Seokheun Choi[1,2,3,*]

[1]Bioelectronics & Microsystems Laboratory, Department of Electrical & Computer Engineering, State University of New York at Binghamton, Binghamton, NY 13902, USA

[2]Center for Research in Advanced Sensing Technologies & Environmental Sustainability, State University of New York at Binghamton, Binghamton, NY 13902, USA

[3]Lead contact

*Correspondence: sechoi@binghamton.edu

https://doi.org/10.1016/j.isci.2025.112312

SUMMARY

A scalable, cost-effective paper-based organic field-effect transistor platform has been developed for rapid antimicrobial susceptibility testing (AST) of biofilm-forming pathogens. Traditional AST methods are costly, labor-intensive, and slow, with a lack of standardized biofilm models. This system directly tracks protons generated by biofilms, which serve as key indicators of bacterial metabolism under antibiotic exposure. A proton-sensitive PEDOT:PSS channel is employed, where metabolic proton activity de-dopes the transistor, reducing conductivity. The engineered paper substrate facilitates rapid, high-quality biofilm formation, improving assay reliability. The platform was validated on three clinically significant pathogens against front-line antibiotics, providing real-time, quantitative antibiotic efficacy profiles. Integrated with a microcontroller and machine learning algorithm, results are displayed on a liquid crystal display (LCD), classifying antibiotic concentration relative to the minimum inhibitory concentration with over 85% accuracy. This clinically translatable system offers a high-throughput, point-of-care solution for efficient infection management and antibiotic stewardship.

INTRODUCTION

Antimicrobial susceptibility testing (AST) is a critical component of modern healthcare, guiding the selection of effective treatments that minimize adverse outcomes and associated costs.[1,2] Precise AST enables the identification of narrow-spectrum antibiotics tailored to specific infections, thereby preserving the beneficial human microbiome and mitigating detrimental immune responses.[3,4] The key to this process is determining the appropriate antibiotic dosage, specifically the minimum inhibitory concentration (MIC), to eliminate target pathogens while ensuring patient safety and preventing collateral organ damage.[5–7] The urgency for advanced AST methods has intensified as antimicrobial resistance emerges as a leading global health threat, projected to cause up to 10 million deaths annually by 2050 if unaddressed—surpassing cancer mortality rates.[2,8,9] Without timely AST guidance, clinicians may resort to prescribing broad-spectrum antibiotics or subtherapeutic doses, allowing pathogens to survive, adapt, and develop resistance.[10,11] Despite the significant contribution of large-scale antibiotic misuse in agriculture, aquaculture, and environmental management to rising resistance, immediate impact can be achieved through appropriate antibiotic use in healthcare settings.[12–14] The World Health Organization identifies these environments as critical hotspots for the emergence and dissemination of multidrug-resistant pathogens, often leading to severe conditions such as bloodstream infections, pneumonia, and surgical site infections.[15,16] While efforts to reduce antibiotic resistance in those large-scale sectors may take years to manifest due to environmental dispersion, targeted interventions—such as antibiotic stewardship programs and focused application of AST within healthcare settings—have demonstrated rapid and direct reductions in resistance levels, highlighting their immediate effectiveness.[17]

Despite the essential role of AST in guiding evidence-based, narrow-spectrum antibiotic prescribing, conventional AST protocols face significant limitations that impede timely and accurate clinical decision-making.[18–20] Those methods are inherently slow, costly, and labor-intensive, requiring extended microbial growth in the presence of antibiotics to determine effective treatments. That heavy dependence on pathogen growth and replication rates inherently delays results, leading to worsened patient outcomes and increased healthcare costs. Moreover, the reliance on specialized, bulky, and non-portable equipment makes those methods impractical for rapid or on-site analysis, often compelling clinicians to prescribe empirical broad-spectrum antibiotics without prior AST.[20] Such practices can lead to unnecessary or inappropriate prescriptions, thereby promoting the

development of antibiotic resistance mechanisms.[21] In addition, conventional AST techniques focus on individual bacteria in their planktonic form, failing to replicate real-world clinical scenarios involving biofilm-associated infections, which constitute 65–80% of pathogenic encounters.[22–25] Biofilms exhibit significantly higher resistance to antibiotics, rendering MIC values effective for planktonic cells subtherapeutic for biofilm-embedded bacteria.[25] That inadequate dosing fails to eliminate biofilms and promotes the development of antibiotic resistance within those resilient microbial communities.[26] Therefore, conventional AST methods, hindered by slow processing, high costs, labor intensity, lack of portability, and an exclusive focus on planktonic bacteria, fail to deliver timely, effective treatments and fall short in addressing the complex resistance mechanisms of real-world infections, exposing a critical gap in current testing protocols.

Herein, we introduce a rapid and sensitive phenotypic AST platform that employs an easy-to-use, cost-effective papertronic approach specifically designed for clinically significant biofilm-forming pathogens (Figure 1). By amplifying the electrochemical signals of bacterial metabolic activity using an organic field-effect transistor, our system enables the evaluation of antibiotic susceptibility significantly earlier than conventional culture methods—even before bacterial populations become detectable. Unlike traditional AST methods that rely on substantial bacterial proliferation to achieve measurable turbidity, our transistor responds to metabolic proton generation, thereby providing susceptibility information at early time points—often well before significant growth is detectable by standard optical density measurements or plating. Using specialized microbial redox mechanisms, specifically the respiratory generation of protons, this platform delivers real-time insights into antibiotic efficacy, significantly expediting clinical decision-making processes. The papertronic organic transistor system is central to this system (Figures 1A and 1B), offering a sustainable, affordable, disposable, and scalable solution for bioelectronics and biosensing. Fabricated using straightforward techniques such as wax printing, microfluidic patterning, and thermal treatment, the device combines precision with low production costs, making it ideal for point-of-care applications. Moreover, the integration of a paper-based culturing system within the papertronic device facilitates rapid biofilm formation that accurately replicates the three-dimensional *in vivo* environment. This capability is crucial as biofilms present unique challenges in antibiotic resistance; our system's ability to model these complex structures provides a more relevant and predictive susceptibility assessment. The transistor channel is engineered with p-type poly (3,4-ethylenedioxythiophene) sulfonate (PEDOT:PSS), where the strong wicking properties of the modified paper enhance cell adhesion and promote biofilm formation upon the introduction of bacterial samples. Under a negative gate voltage, additional hole charge carriers are attracted to the channel (Figure 1B). However, the predominant generation of protons from bacterial metabolic activity triggers a de-doping process within the PEDOT:PSS channel, leading to a reduction in the overall current (Figures 1C and 1D). Simultaneously, the majority of metabolically produced electrons are diverted due to their interaction with oxygen. In the presence of effective antibiotics, bacterial metabolism, and proton production decrease, diminishing the degree of de-doping and slowing the rate of current reduction (Figure 1D). This change in electrical behavior provides a measurable indicator of antibiotic susceptibility. By employing the transistor as a biosensor, weak bioelectrical signals are amplified as small metabolic changes regulate a larger current flow, enabling the detection of subtle variations in bacterial activity that would otherwise be undetectable. This platform marks a transformative leap in AST, delivering rapid, on-site diagnostics with minimal resource demands while improving accessibility across diverse healthcare environments. By unraveling the interaction between bacterial metabolic activity under antibiotic exposure and organic transistors within the paper-based culturing system, it empowers more responsive and effective infection management, particularly in addressing the formidable challenges of biofilm-associated antibiotic resistance. Although certain automated AST systems can yield results in 4–6 h, our paper-based platform is designed to be low-cost, portable, and capable of modeling biofilm conditions in a simple format, making it well-suited for resource-limited settings or routine lab use without large instrumentation.

RESULTS

Operating principle of the paper-based organic transistor for antimicrobial susceptibility testing

Microbial respiration involves a series of electron transfers through an electron transport chain, during which the energy released is used to pump protons, establishing an electrochemical proton gradient across the cell membrane.[27] This gradient is critical, as it stores the potential energy required for synthesizing adenosine triphosphate (ATP), the primary energy carrier that supports microbial viability. While microbial respiration is typically aerobic, utilizing oxygen as the final electron acceptor, anaerobic respiration can also occur, relying on alternative acceptors.[27,28] Certain microorganisms possess the unique capability to transfer electrons extracellularly to external solid electrodes, serving as their final electron acceptor. Previously, our group pioneered an innovative method to monitor extracellular electron transfer as a rapid and reliable indicator of microbial metabolic activity in response to antibiotics.[29] However, those techniques were limited to specific exoelectrogenic pathogens, and the electrical signals generated were insufficient to deliver reliable and sensitive measurements of MICs.[30]

While monitoring extracellular electron transfer has many limitations, monitoring metabolically produced protons can be a more general method not limited by bacterial type. Various techniques employing nuclear magnetic resonance (NMR) spectroscopy, fluorescent dyes, and pH indicators have been demonstrated to monitor proton production in response to antibiotics.[31–33] However, NMR spectroscopy is bulky, expensive, and unsuitable for on-site measurements, while techniques using fluorescent dyes and pH indicators are highly susceptible to environmental factors that can affect their accuracy and reliability. Moreover, the outputs of these measurement systems are not electrical signals, making them difficult to analyze and less practical for on-site antibiotic prescription. Recently, protons have been electrically detected using ion-sensitive field-effect transistors (ISFETs) that utilize HfO_2 as a selective material

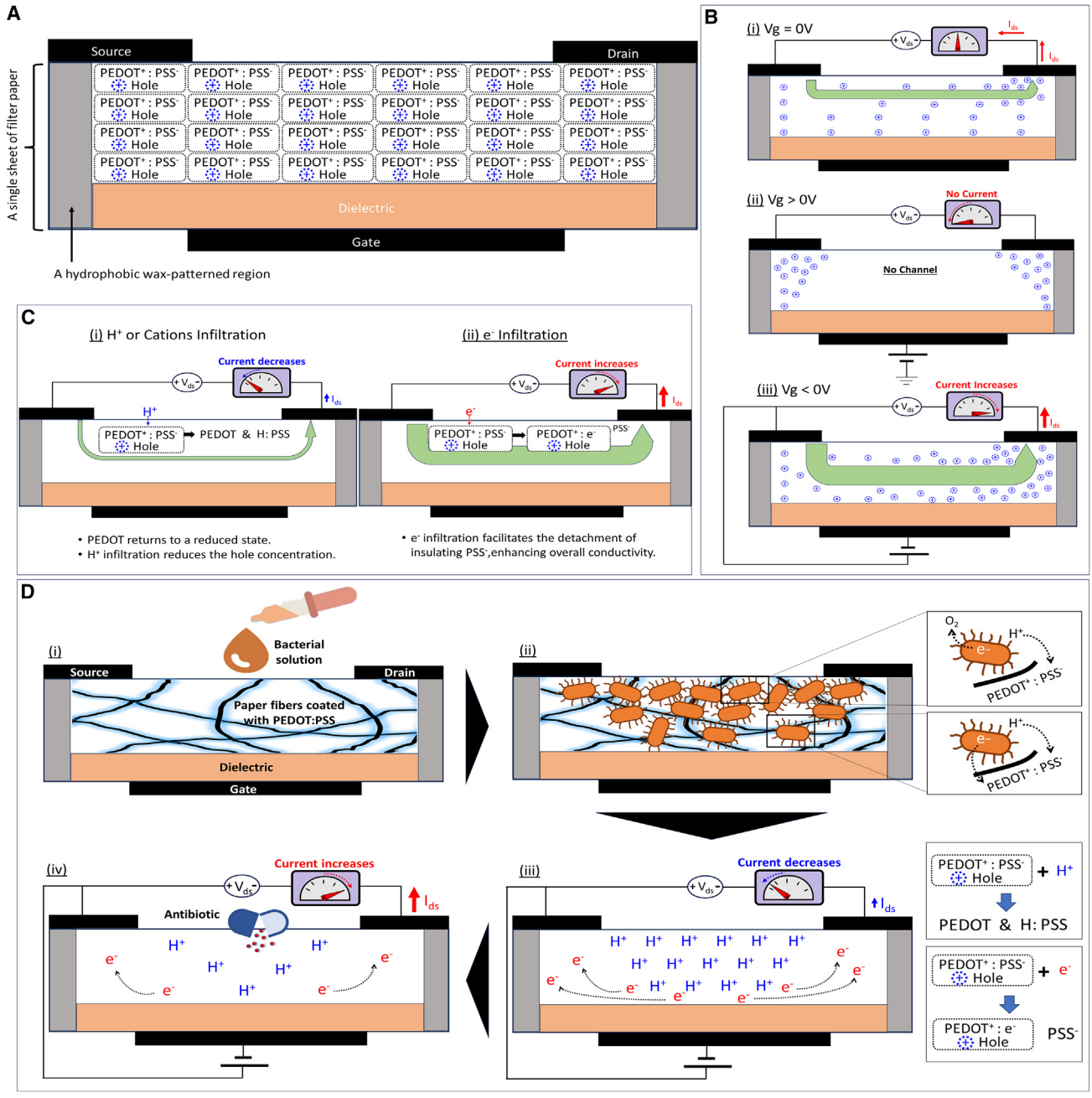

Figure 1. Operating principle of the paper-based organic transistor for AST

(A) Configuration of the field-effect transistor using PEDOT:PSS as its active channel material.

(B) General working mechanism of the p-type PEDOT:PSS transistor under varying gate voltages: (i) Vg = 0, (ii) Vg > 0, and (iii) Vg < 0.

(C) Modulation of transistor current as a function of proton/cation or electron infiltration, showcasing its sensitivity to ionic and electronic transport.

(D) AST mechanism using the transistor-based sensor: (i) introduction of pathogen-containing samples to the sensor, (ii) biofilm formation and metabolic activity of pathogens, producing protons and electrons, (iii) Modulation of conductivity under transistor operation, driven by proton and electron generation, and (iv) Current modulation as a measurable response to antibiotic exposure, enabling real-time AST evaluation.

for proton detection.[34] However, challenges such as thermodynamic instability and limited selectivity have compromised the long-term reliability and effectiveness of these sensors. Moreover, inconsistencies in the deposition of HfO_2 layers and variations in operating conditions can lead to fluctuations in sensor performance.

Here, we introduce an innovative proton detection mechanism by leveraging conventional organic electrochemical field-effect

transistors (OFET) that utilize conducting polymers as channels. While traditional transistors modulate channel conductivity through doping or de-doping with ions migrating from the electrolyte-based dielectric under an applied gate voltage,[35,36] the channel conductivity of our device is directly modulated by protons produced from microbial metabolism within the channel where the bacterial sample is introduced. In this study, the widely used conductive polymer PEDOT:PSS was employed as the channel material, while polyvinyl alcohol (PVA) served as a solid-state electrolyte to form the field-effect transistor. However, it is challenging to classify this device as an OFET, because that typically uses electrolytes with a high ion content to modulate the channel conductivity. When PEDOT interacts with PSS, the PEDOT chains become positively doped due to the withdrawal of electrons from the polymer backbone.[37] The resulting positive charges (oxidized $PEDOT^+$) are balanced by the counter anion PSS^-, forming an overall neutral state. Despite this neutrality, the ionic interaction causes the delocalization of charge carriers, "holes," along the PEDOT backbone and serve as current carriers (Figure 1A).[38,39] Consequently, even at zero gate voltage (*Vg*), applying a source-drain voltage induces a source-drain current, and the transistor operates in depletion mode (Figure 1B (i)).[40] When a positive gate voltage is applied, holes are depleted from the channel, reducing the current flow (Figure 1B (ii)). Conversely, a negative gate voltage attracts more holes to the channel, facilitating an increase in source-drain current (Figure 1B (iii)). In this latter state, protons or cations externally introduced by bacterial metabolism interact with PEDOT:PSS, effectively neutralizing the negatively charged PSS chains, returning PEDOT to its reduced state (Figure 1C (i)).[41,42] This reduction lowers the overall hole concentration in the channel, thereby decreasing the source-drain current. Conversely, the introduction of electrons can alter the material by potentially initiating the detachment of PSS and interacting with the positively charged $PEDOT^+$ (Figure 1C (ii)).[43,44] This process mimics the effect of adding organic solvents such as dimethyl sulfoxide (DMSO) or ethylene glycol (EG) to PEDOT:PSS, where the insulating PSS is removed, leading to an increase in the conductivity of PEDOT:PSS.[39,45] Moreover, as more electrons readily interact with $PEDOT^+$, the delocalization of electrons along the polymer backbone is significantly enhanced, improving the conductivity of the channel. Those additional electrons can participate in forming bipolarons—pairs of charge carriers—that further enhance conductivity by establishing more conductive pathways. The addition of PSS makes PEDOT water-dispersible and stable in a liquid-state solution,[37] enabling easy conductive coating of non-conductive paper fibers through wicking into the hydrophilic paper (Figure 1D (i)).[46] This process results in a thin, uniform, and conformal deposition of the PEDOT:PSS material over the paper fibers, preserving the paper's original morphology and leaving its pores unblocked.[46–48] This enables bacterial cells to move freely, form biofilms, and efficiently access nutrients, and is extensively documented in our previous studies.[47–49] Most of the electrons generated by bacterial metabolism are diverted to interact with oxygen in the air, serving as a terminal electron acceptor (Figure 1D (ii)).[28] While microbial extracellular electron transfer (EET) mechanisms can deliver electrons to PEDOT:PSS deep within the biofilm, effectively blocking oxygen invasion into the biofilm,[47,48] the application of a negative gate potential repels these electrons from the channel (Figure 1D (iii)). This repulsion prevents the electrons from contributing to the formation of conductive pathways within the channel, thereby limiting their ability to enhance the overall conductivity.

Our innovative working principle was validated through two distinct experimental setups: aerobic and anaerobic environments (Figure 2). Protons and electrons arise from the bacterium's metabolic respiration. We have confirmed that adjusting the pH in control experiments similarly changes the channel conductivity, supporting that protons indeed de-dope PEDOT:PSS. In the aerobic condition, which served as the primary experimental scenario, significant current reduction was observed during bacterial biofilm formation (Figure 2A). This finding suggests that metabolically produced protons act as primary doping agents that reduce the number of positive charges on PEDOT chains, thereby decreasing the channel's overall conductivity (Figure 1C (i)). Concurrently, electrons are either consumed by oxygen or repelled by the applied gate voltage, further contributing to the current decrease. In contrast, under anaerobic conditions where oxygen is absent, both metabolically produced electrons and protons influence the transistor channel's conductivity (Figure 2B). While protons reduce conductivity by de-doping the polymer, electrons enhance conductivity by increasing delocalization along the polymer backbone (Figure 1C (ii)). In our experiments, the biofilm's metabolic activity generated a surplus of electrons compared to protons, leading to an overall increase in channel conductivity. These contrasting results highlight the intricate interplay between biofilm metabolism and transistor behavior, underscoring the pivotal role of environmental conditions in shaping the electrical response of the system. However, our PEDOT:PSS channel is primarily modulated by metabolically produced protons under aerobic conditions, which decrease the current flow by compensating for the positive charges in the PEDOT chains (Figure 1D). Therefore, our transistor sensitively and rapidly monitors microbial metabolic activity by primarily detecting protons produced during cellular metabolism. This proton monitoring makes the device highly effective in responding to antibiotics (Figure 1D (iv)). Increased microbial activity leads to elevated proton production, which compensates for the charge carriers in the channel, resulting in a greater reduction of the source-drain current. When microorganisms are susceptible to antibiotics, their metabolic activity decreases due to the inhibitory effects of the drugs. This reduction in activity leads to lower proton production, minimizing the current reduction in the transistor. Conversely, when pathogens are resistant to antibiotics, their metabolic activity remains unaffected. This sustained activity causes significant proton production, leading to substantial current reduction due to the extensive compensation of holes in the channel. The ability to detect these changes in real time allows for the rapid assessment of antibiotic efficacy. Although proton-mediated de-doping is the predominant mechanism, we recognize that other ions, such as potassium and sodium, may also contribute to modulating the local doping state of PEDOT:PSS, especially under complex metabolic conditions. Further studies are needed to fully investigate the influence of these cations.

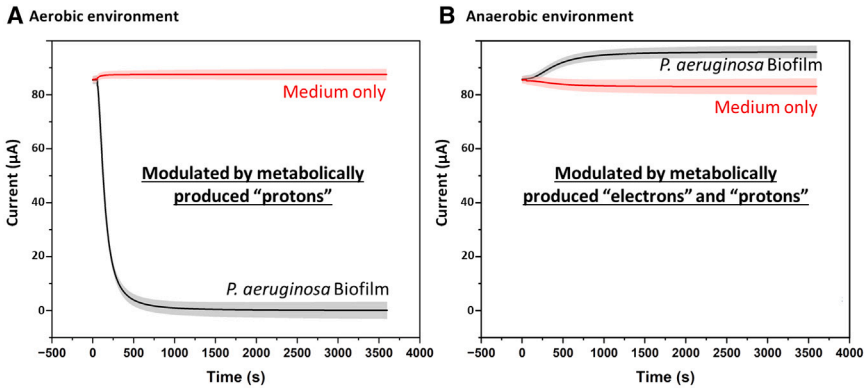

Figure 2. Validation of the working principle

(A) In an aerobic environment, the current output of the organic transistor significantly decreases as metabolically produced protons from the P. aeruginosa biofilm become the primary charge carriers. These protons de-dope the PEDOT:PSS channel, reducing its conductivity. Meanwhile, metabolically produced electrons are either consumed by oxygen in the air or repelled by the applied gate voltage.

(B) In an anaerobic environment, both electrons and protons affect the conductivity of the transistor channel. However, electrons play a more substantial role, increasing delocalization along the polymer backbone and ultimately leading to an overall enhancement in channel conductivity. (The shaded area represents the standard error of the experimental replicates.).

A paper-based organic transistor integrated into a fully papertronic circuit system

Recently, our group pioneered a new papertronic technique that addresses the long-standing challenges posed by paper's porosity, which had previously hindered the fabrication and performance of electronic components.[50,51] This innovative approach leverages paper's inherent capillary action, enhanced by hydrophobic wax patterning, to enable precise vertical integration of electronic components—a notable advancement beyond conventional surface deposition methods. Using this technique, we successfully developed organic n-type and p-type transistors employing perylene bis(dicarboximide) (PDI) and 6,13-bis(triisopropylsilylethynyl) pentacene (TIPS pentacene), respectively.[51] In this study, TIPS pentacene has been replaced with PEDOT:PSS because of its exceptional electrical conductivity, mechanical flexibility, and tunability through doping and de-doping processes,[37,38] aligning seamlessly with our AST mechanism for sensitively detecting metabolic proton generation.

Figures 3A and 3B depict the distinctive architecture of the transistor, characterized by the gate electrode located on the bottom surface of the paper substrate, while the source and drain electrodes, along with the bacterial sample introduction channel, are positioned on the top surface. The fabrication process begins with defining the transistor's area using a double-sided wax printing technique applied to both sides of the paper (Figure S1A). Thermal treatment is then employed to ensure the wax penetrates the substrate and solidifies effectively. Subsequently, a PVA-based dielectric ink, dissolved in deionized (DI) water, is deposited on one side of the paper via inkjet printing. The ink's penetration is precisely controlled to approximately half the paper's thickness, a result of the balance between its viscosity and the natural capillary action of the paper. On the opposite side, PEDOT:PSS solution is deposited through inkjet printing, which wicks downward until it interfaces with the upper boundary of the PVA dielectric layer. This process results in the fibers of the paper being coated with both PVA and PEDOT:PSS, providing a suitable substrate for the deposition of electrode materials. The gate electrode is subsequently deposited on the bottom surface, while the source and drain electrodes are formed on the top surface. The material integration and the layered structure of the transistor are confirmed using optical microscopy and scanning electron microscopy (SEM), as presented in Figure 3C. These imaging techniques reveal a stratified architecture, with the PVA dielectric and the channel each measuring approximately 170 μm in thickness, within a total paper thickness of 340 μm. Additionally, electrodes with a uniform thickness of approximately 50 μm are deposited on both the top and bottom surfaces. This consistency underscores the precision and reproducibility of the fabrication method, demonstrating its potential for scalability and practical implementation in advanced applications. The transfer characteristics and output curves exhibit typical field-effect transistor behavior of a p-type semiconductor active layer, where the source-drain current is regulated by the gate-source voltage (V_g) (Figures S1B and S1C). The transistor demonstrates a hole mobility of 4×10^{-2} $cm^2/V \cdot s$ and an on/off current ratio (I_{on}/I_{off}) of approximately 5.5×10^3 at a low operating voltage of −2 V. The output characteristics display excellent linear behavior, clear saturation, and significant field-effect current modulation. At $V_{gs} = 0$, a drain current flows due to the high conductivity of PEDOT:PSS with holes as charge carriers, indicating that the transistor operates in depletion mode. Applying a positive V_{gs} decreases the drain current as holes are depleted within the channel. However, even at higher V_{gs}, the drain current is not completely depleted because the thick dielectric layer hinders effective gate modulation.[52] Additionally, trap states, interface effects, and inherent material properties may contribute to the incomplete depletion of the PEDOT:PSS channel.[53,54] Despite this limitation, operating the transistor with V_{gs} set to negative values while maintaining the drain-source voltage (V_{ds}) at a sufficient level ensures operation in the saturation region, thereby optimizing sensitivity for accurately monitoring bacterial metabolic activity. Consequently, the incomplete depletion does not adversely affect our biosensing performance.

To operate the p-type transistor effectively in a more systematic manner, a circuit was designed using three paper resistors on a paper-based printed circuit board (PCB), forming a fully integrated papertronic system (Figure 3D). A DC power supply (Vss = 15 V) was introduced as the operating voltage for the gate and source after 1 h of cultivation. A 1 MΩ resistor connected to the gate ensures that the gate voltage remains lower

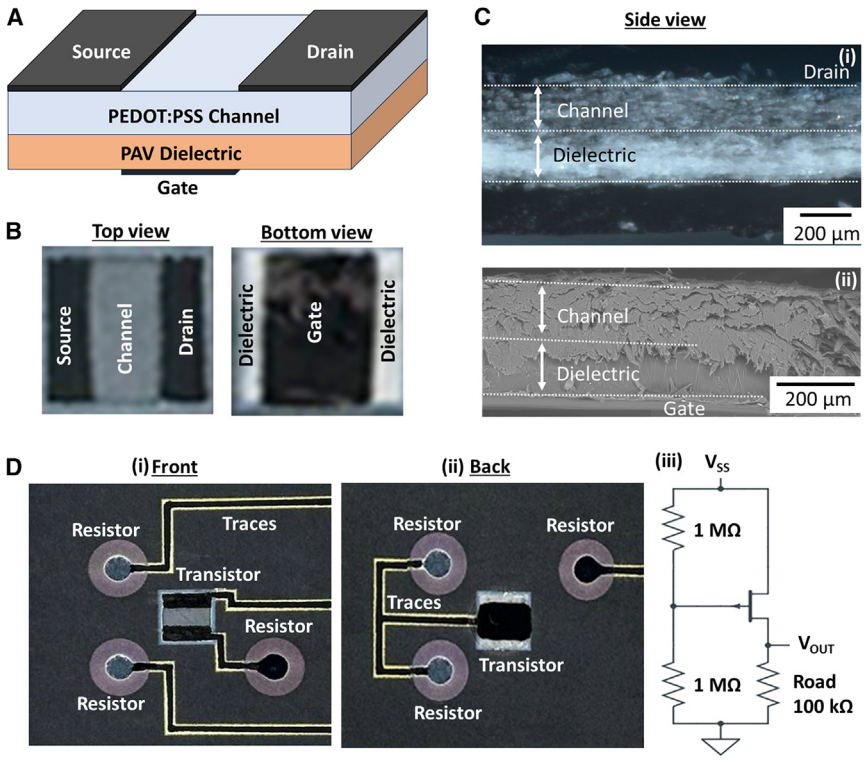

Figure 3. A paper-based organic transistor and its integrated papertronic circuit system

(A) Schematic diagram of the paper-based organic transistor.

(B) Photographs showing the top and bottom views of the transistor.

(C) Cross-sectional images of the transistor: (i) microscopic view and (ii) SEM view.

(D) Photographs of the papertronic circuit system used to operate the transistor: (i) front view and (ii) back view, accompanied by (iii) the circuit diagram detailing all components.

than the source voltage. Additionally, another 1 MΩ resistor, along with a 1 kΩ load resistor, is incorporated into the circuit to ensure that the transistor operates within the saturation region. The resistor values are adjusted by varying the amount of diluted PEDOT:PSS in DI water; resistances of 1 MΩ and 1 kΩ are achieved using 3 μL and 6 μL of a 50% PEDOT:PSS solution, respectively (Figure S1D). For the conductive traces on the paper-based PCB, a composite of graphene and PEDOT:PSS is used.[51] Graphene's extensive surface area and its capability to improve polymer matrix properties—such as electrocatalytic efficiency, mechanical strength, and thermal performance—make graphene-PEDOT composites an excellent choice for metallic wires in PCBs.

Enhanced biofilm growth in paper-based channels

Developing reliable models that rapidly form complex and diverse biofilms is critical for monitoring antibiotic efficacy against biofilm-associated infections and understanding the increased resistance of biofilms to antibiotics.[23–26] Despite this need, there are no universally standardized models that enable simple, rapid, reliable, and effective biofilm formation and development. In this context, we present an innovative approach using the paper-based channel of the organic transistor as a supportive 3D cell culture platform. This platform replicates the structural, functional, and physiological characteristics of bacterial biofilms while enabling swift and reliable monitoring of bacterial metabolism through microbial proton production measurements. Our paper-based channel simulates the highly porous structure of natural microbial environments, facilitating adequate nutrient exchange to sustain internal bacterial colony growth and the development of dense multilayer biofilms. The strong capillary action of the paper-based channel enables rapid cell adsorption, leading to the formation of densely packed aggregates. This high cell density enhances bacterial communication via quorum sensing,[48,55,56] expediting biofilm formation compared to the days-long or weeks-long timelines of conventional techniques. Our recent studies demonstrate that biofilms can be rapidly formed on this paper platform, with a quality comparable to the complex and diverse 3D biofilms produced by traditional dynamic and static *in vitro* models—which are often labor-intensive, costly, time-consuming, and equipment-dependent.[30,57] This breakthrough not only advances biofilm modeling but also allows integration into the channel component of the organic transistor, enabling it to function dually as both an *in vitro* biofilm model and a metabolic proton monitor. This dual functionality offers an innovative approach for biofilm-forming AST.

In previous studies, we observed that the paper-based culture platform could develop a high-quality *P. aeruginosa* biofilm using its culturing sample with an optical density at 600 nm (OD_{600}) of 1.0—equivalent to approximately 10^9 CFU/mL—after just 1 h of cultivation.[30] An OD_{600} of 1.0 is an optimal concentration that can be achieved in just 6 h using a regular culture, allowing for the rapid formation of a high-quality biofilm suitable for subsequent AST. While extended cultivation times result in thicker and more densely packed biofilms (Figures 4 and S2), a 1-h culture at an OD_{600} of 1.0 is sufficient to form a biofilm with extracellular polymeric substances (EPS) encapsulating the bacterial cells. This was comprehensively demonstrated through SEM imaging in this study and further supported by EPS protein measurements in our previous work.[30]

Furthermore, quantitative biofilm formation was rigorously evaluated using our previously developed microbial fuel cell technique, which clearly demonstrated a direct correlation between bacterial electrogenic output and the progression of biofilm development (Figure S3).[30,56,57] Notably, even low bacterial concentrations, such as OD_{600} values of 0.1, 0.2, 0.5, and 0.7, were capable of achieving comparable biofilm formation with extended cultivation times (Figures 4 and S3). For example, a

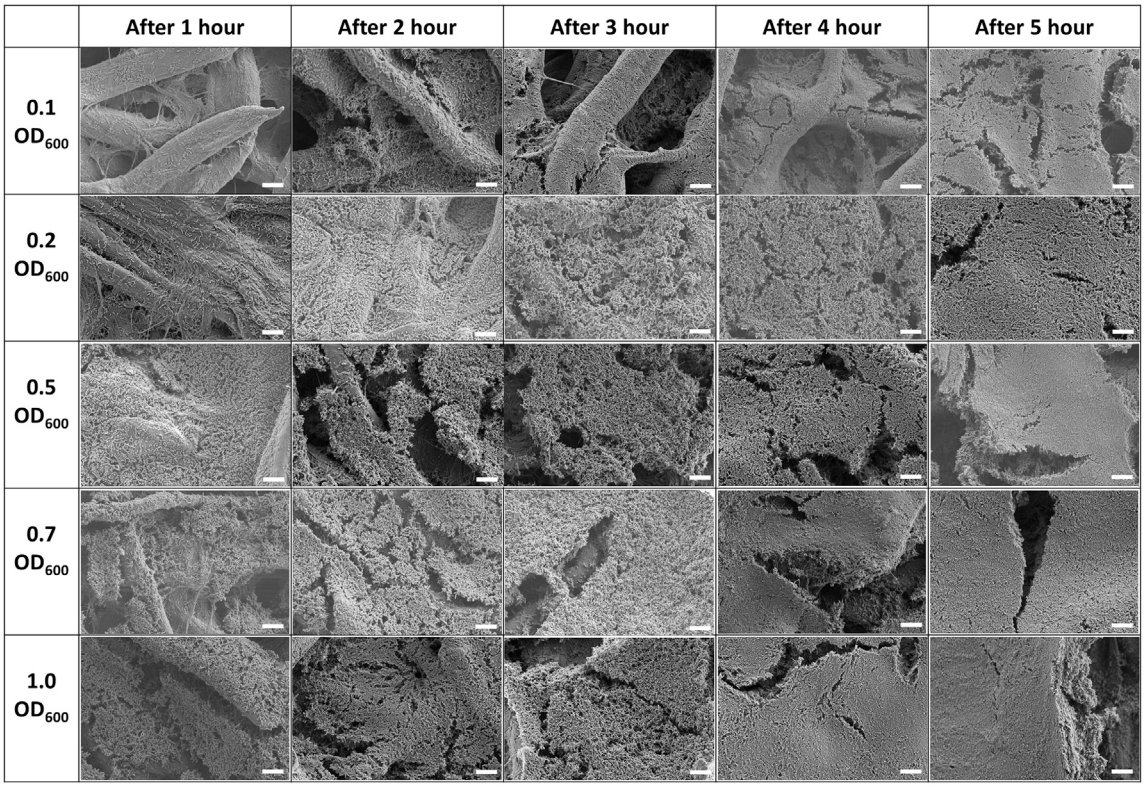

Figure 4. Visualization of *P. aeruginosa* biofilm formation within the paper-based transistor channel

SEM images depict biofilms formed using various initial bacterial concentrations at different cultivation time points. (White scale bar: 10 μm).

culture at 0.1 OD_{600} (~10^8 CFU/mL), equivalent to the ~0.5 McFarland turbidity standard commonly used in conventional phenotypic ASTs, required over 9 h of cultivation to match the biofilm quality formed within 1 h at an OD_{600} of 1.0. These findings underscore the potential of our paper-based model as a transformative tool for studying pathogenic biofilms, even with low concentrations of clinical samples.

Electrical profiling of antibiotic susceptibility

In this study, we evaluated the efficacy of three frontline antibiotics—gentamicin (GEN), ciprofloxacin (CIP), and cefotaxime (CEF) —against three clinically significant pathogens: *Pseudomonas aeruginosa*, *Escherichia coli*, and *Staphylococcus aureus*. These antibiotics were selected due to their fundamentally different mechanisms of action: GEN inhibits protein synthesis by binding to the 30S ribosomal subunit; CIP impedes DNA replication by inhibiting DNA gyrase activity, and CEF disrupts cell wall synthesis by preventing the formation of peptidoglycan.[58] *P. aeruginosa* is a Gram-negative opportunistic pathogen known for causing serious and life-threatening infections, especially in immunocompromised individuals.[59] It exhibits exceptional and complex mechanisms of antibiotic resistance, including efflux pumps and enzymatic degradation, making it a significant threat in clinical settings. The ability of *P. aeruginosa* to form biofilms—a structured community of bacteria embedded in a self-produced extracellular matrix—further exacerbates its resistance, leading to treatment challenges and persistent infections. Similarly, Gram-negative *E. coli* is a leading cause of urinary tract infections, bloodstream infections, and other human diseases.[60] It can develop multiple mechanisms of antibiotic resistance, such as beta-lactamase production and alterations in target sites. The formation of biofilms by *E. coli* significantly contributes to its pathogenicity, particularly in urinary tract infections, catheter-associated infections, and medical device-related infections. Gram-positive *S. aureus* is one of the most virulent pathogens, responsible for a wide range of clinical diseases, from skin infections to life-threatening conditions such as sepsis.[61] It exhibits various mechanisms of antibiotic resistance, notably through the acquisition of resistance genes such as mecA, which confers methicillin resistance. In the clinical context, biofilm-forming *S. aureus* is a major concern for infections associated with implanted medical devices, such as prosthetic joints and catheters, due to its increased resistance to antibiotics and the host immune response. Our transistor-based AST platform provides valuable phenotypic information for a quantitative understanding of antibiotic effectiveness and mechanisms of action. Changes in antibiotic efficacy, concentration, and mode of action affect the doping degree of the PEDOT:PSS channel in our device, thereby altering the magnitude of the source-drain current outputs. This correlation enables real-time monitoring of bacterial responses to antibiotics, facilitating rapid and accurate AST.

Initially, the transistor channels were inoculated with individual bacterial species at a concentration corresponding to an OD_{600} of 1.0. The devices were then incubated for 1 h to allow for initial

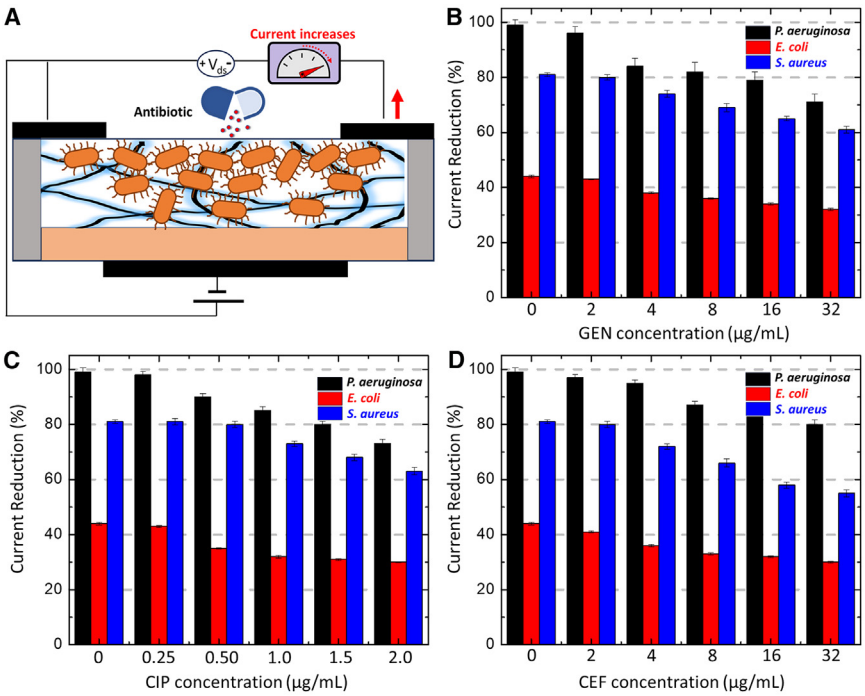

Figure 5. Antibiotic susceptibility profiling of biofilms formed by three pathogens (*P. aeruginosa*, *E. coli*, and *S. aureus*) exposed to three antibiotics: GEN, CIP, and CEF

(A) Schematic illustration of the test setup.

(B–D) Percentage reduction in transistor current with increasing concentrations of (B) GEN, (C) CIP, and (D) CEF, demonstrating antibiotic response profiles.

biofilm formation on the PEDOT:PSS channel surfaces. Following this incubation, antibiotics at varying concentrations were introduced into the system (Figure 5A). The cultures were further incubated for an additional 1 h to facilitate interaction between the bacteria and the antibiotics. The metabolic activity of the bacteria results in the production of protons, which leads to the de-doping of the PEDOT:PSS channel. This de-doping process decreases the electrical conductivity of the channel. We monitored these conductivity changes by measuring the voltage drop across a load resistor connected in series with the transistor channel (Figure 3D (iii)). The alterations in the voltage drop provide a real-time, quantitative measure of bacterial response to the antibiotics, reflecting changes in bacterial viability and metabolic activity due to the antibiotic treatment. This approach allows for the assessment of antibiotic effectiveness and the elucidation of their mechanisms of action based on phenotypic responses. Notably, the metabolic activity of bacteria varies significantly depending on the species, resulting in distinct effects on channel conductivity (Figures 5 and S4). Among the tested pathogens, *P. aeruginosa* exhibited the most pronounced metabolic activity, leading to a substantial voltage drop across the load resistor, reducing it nearly to zero (Figure S4). This indicates an almost complete reduction of PEDOT, effectively halting current flow through the channel. Following *P. aeruginosa*, *S. aureus* demonstrated intermediate metabolic activity, resulting in a moderate voltage drop. *E. coli*, in contrast, exhibited the lowest metabolic activity, corresponding to the smallest impact on channel conductivity. These differences underscore the species-dependent metabolic response and its influence on the electronic properties of the PEDOT:PSS channel, offering valuable insights into bacterial behavior and their interaction with the sensing platform.

The introduction of antibiotics to the pathogenic biofilms significantly reduced bacterial metabolic activity, with the extent of this reduction varying across species. Among the tested antibiotics, GEN induced a rapid and pronounced voltage drop for *P. aeruginosa*, followed by *E. coli* (Figure S4). In contrast, *S. aureus* exhibited a slower and more gradual response to GEN, indicating species-specific variations in susceptibility and metabolic adaptation to the antibiotic. Despite these differences in response rates, all bacterial species showed negligible voltage drops at a GEN concentration of 2 μg/mL. However, a noticeable and substantial voltage drop was observed at a concentration of 4 μg/mL, which can be defined as the MIC for this antibiotic. This MIC value reflects the threshold at which GEN effectively inhibits bacterial metabolic activity across the tested species. The MIC value was determined as the lowest antibiotic concentration that prevented a further significant voltage drop ($\leq$10% of the drop observed in antibiotic-free controls). This threshold was consistent with standard definitions of growth inhibition observed in conventional culture-based AST.[30,56] CIP exhibited the greatest effectiveness against *E. coli* biofilms, eliciting the most rapid response with an MIC value of 0.5 μg/mL (Figure 5C). In contrast, *P. aeruginosa* and *S. aureus* responded more slowly (Figure S4), with MIC values of 0.5 μg/mL and 1 μg/mL, respectively (Figure 5C). These results highlight the pronounced efficacy of CIP against *E. coli* biofilms compared to those formed by other species. In the case of CEF, all three bacterial species exhibited unusual response profiles characterized by an initial steep voltage drop, followed by a gradual recovery in voltage (Figure S4). Among the tested species, *E. coli* demonstrated the highest sensitivity, with an MIC value of 2 μg/mL (Figure 5D). Both *P. aeruginosa* and *S. aureus* displayed higher MIC values of 4 μg/mL, indicating reduced susceptibility to CEF under the experimental conditions. These findings underscore the capability of our transistor-based platform to detect species-specific responses to antibiotics with high sensitivity by monitoring changes in electrical conductivity linked to bacterial metabolism. The observed differential responses to antibiotics among the bacterial species emphasize the importance of tailoring antibiotic susceptibility testing to individual microbial characteristics. Additionally, the platform's ability to accurately determine

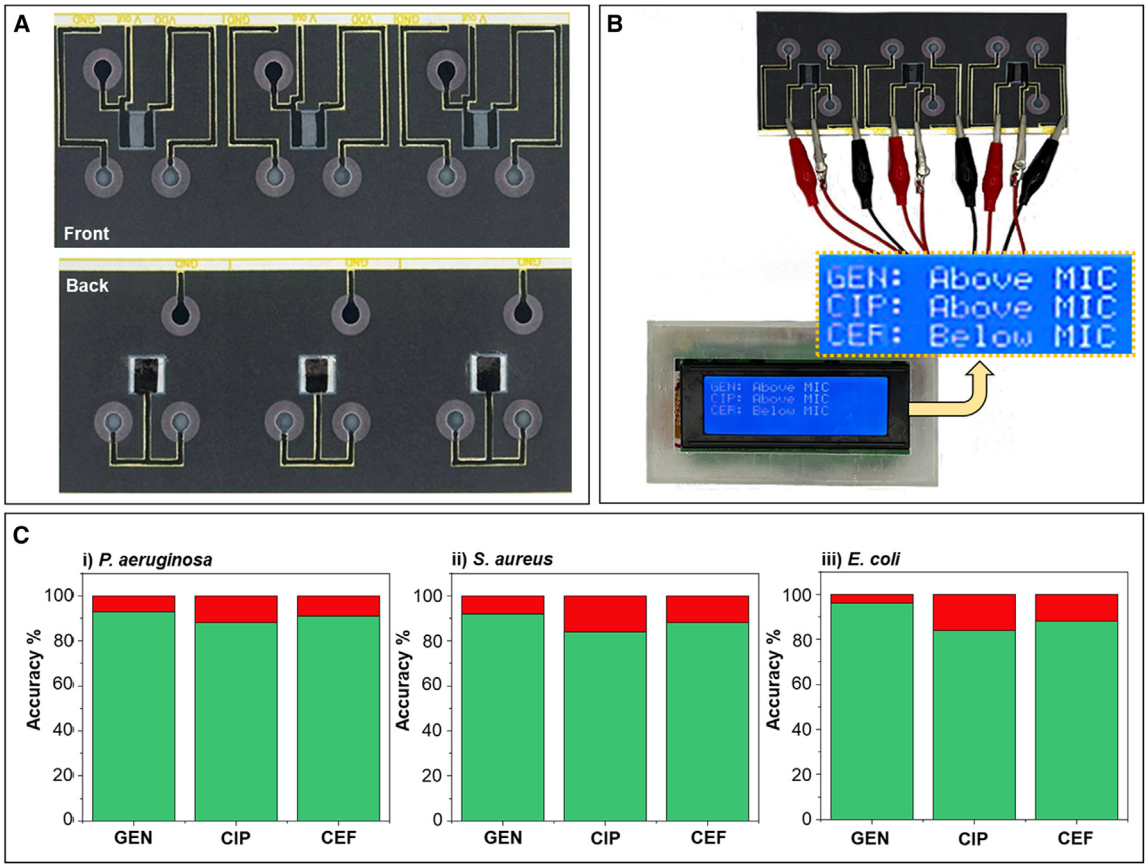

Figure 6. A paper-based organic transistor and integrated papertronic circuit system for AST

(A) Schematic representation of the paper-based organic transistor array.

(B) Point-of-care operation of the AST system, showcasing its functionality in determining whether the tested antibiotic concentration is below, above, or at the MIC for the target pathogen.

(C) System accuracy demonstrated through blind testing with unknown antibiotic samples.

MIC values highlights its potential as a rapid and reliable tool for evaluating antibiotic efficacy in clinical diagnostics.

Our innovative papertronic platform provides a scalable and efficient solution for high-throughput biosensing, demonstrating transformative potential for AST. In this study, we seamlessly integrated three AST sensors onto a single sheet of paper, creating a compact, cost-effective configuration (Figure 6A). These sensors were coupled with a custom-designed readout system programmed via Arduino Duo microcontrollers. The system processes data and displays results on a liquid crystal display (LCD), indicating whether the tested antibiotic concentration is below, above, or at the MIC value for the target pathogen (Figure 6B). To validate the platform's accuracy and practical utility, we conducted blind testing with unknown antibiotics. A machine learning algorithm, specifically the mean square error (MSE) algorithm, was embedded into the microcontroller. This algorithm was trained on output signals from the AST sensors and compared the unknown samples' signals against stored reference data to identify the antibiotic used and determine its efficacy relative to the MIC. Blind tests were performed with those three pathogens. For *P. aeruginosa*, blind tests with unknown antibiotics were conducted 100 times for each antibiotic, revealing that the percentage results closely matched those obtained after just 25 iterations. Based on this finding, experiments for *S. aureus* and *E. coli* were repeated 25 times under each antibiotic condition. The outcomes are illustrated in percentage form in Figure 6C, providing a clear comparison of antibiotic efficacy across different bacterial strains. All success rates exceeded 85%, underscoring the robustness and reliability of our testing methodology. While the algorithm can classify unknown antibiotics once trained on a particular species, unidentified pathogens would require either prior species knowledge or expanded training across multiple bacterial species. The advanced readout system, integrating Arduino Duo microcontrollers and the MSE algorithm, represents a powerful tool for identifying antibiotics and determining their effectiveness against specific pathogens. Although we demonstrated three parallel sensors, the paper's large format can be patterned for tens or more sensors, enabling a multi-antibiotic panel akin to commercial systems. Our platform not only simplifies the AST process but also provides real-time, precise data interpretation, making it ideal for point-of-care diagnostics and large-scale clinical applications. While

the current protocol uses pure bacterial cultures, future integration of rapid capture or short enrichment steps could enable more direct testing of clinical specimens, further decreasing the overall time to results.

DISCUSSION

This study introduces an innovative paper-based transistor platform specifically designed for point-of-care AST, with a focus on addressing the challenges posed by biofilm-forming pathogens—a critical need in the global effort to combat antibiotic resistance. Our papertronic device is scalable, sustainable, affordable, and disposable, making it highly suitable for widespread clinical application. The three-dimensional structure and inherent bioaffinity of the paper substrate provide an optimal environment for biofilm formation, closely replicating the structural, functional, and physiological characteristics of bacterial biofilms. Uniquely, the transistor's channel serves a dual purpose: it functions as a sensitive sensing area for monitoring metabolic proton generation and as a culture site that facilitates rapid and high-quality biofilm formation. The p-type PEDOT:PSS channel is highly responsive to protons; metabolic protons produced by bacterial activity de-dope the channel, leading to a measurable reduction in conductivity. This mechanism enables precise, real-time monitoring of bacterial metabolism and viability. We successfully evaluated three clinically significant pathogens—*P. aeruginosa*, *E. coli*, and *S. aureus*—against three frontline antibiotics: gentamicin, ciprofloxacin, and cefotaxime. Our AST sensor provided quantitative profiles of antibiotic effectiveness and mechanisms of action in a rapid, sensitive, and real-time manner. As antibacterial research continues to evolve, integrating emerging technologies such as our papertronic platform will further enhance the capabilities and applicability of AST systems. Our approach represents a significant advancement in developing rapid, accurate, and cost-effective tools to combat antibiotic resistance. By enabling timely and precise antibiotic selection, this technology has the potential to improve clinical outcomes and contribute substantially to public health management.

Limitations of the study

The study presents several limitations that should be considered. First, evaluations were performed using pure bacterial cultures rather than direct clinical samples, which typically contain mixed microbial populations and host-derived factors that may influence results. Future research should include clinical specimens to validate practical utility. Second, the developed machine learning algorithm relies on prior training data for each bacterial species and antibiotic combination, limiting immediate application against unknown or emerging pathogens without extensive preliminary training. Additionally, the platform's sensitivity is primarily based on metabolic proton production; however, other ionic species such as sodium or potassium may also affect the transistor response under varied physiological conditions. Lastly, the platform's robustness under diverse environmental conditions was not extensively assessed, and further investigation is necessary to confirm reliable performance in varied clinical settings and environmental conditions.

RESOURCE AVAILABILITY

Lead contact

Further information and requests should be directed to and will be fulfilled by the lead contact, Seokheun "Sean" Choi (sechoi@binghamton.edu).

Material availability

This study did not generate new unique reagents.

Data and code availability

- All data and code reported in this paper will be shared by the lead contact upon request.
- This paper does not report the original code.
- Any additional information required to reanalyze the data reported in this paper is available from the lead contact upon request.

ACKNOWLEDGMENTS

This study was supported by the National Science Foundation (Grant Nos. 2246975 and 2100757) and the SUNY System Administration through the SUNY Research Seed Grant Award (Grant No. 241000). We gratefully acknowledge the Analytical and Diagnostic Laboratory at SUNY-Binghamton for providing access to their facilities. In preparing this article, we utilized ChatGPT to identify and address grammatical issues, ensuring accuracy through thorough review and subsequent revisions. The authors take full responsibility for the content and conclusions presented in this publication.

AUTHOR CONTRIBUTIONS

Z.R.: Software, methodology, investigation, and formal analysis; M.R.: methodology, investigation, and formal analysis; S.C.: Conceptualization, visualization, writing – original draft, writing – review and editing, and funding acquisition.

DECLARATION OF INTERESTS

The authors declare no competing interests.

STAR★METHODS

Detailed methods are provided in the online version of this paper and include the following:

- KEY RESOURCES TABLE
- EXPERIMENTAL MODEL AND STUDY PARTICIPANT DETAILS
- METHOD DETAILS
  - Bacterial inoculum
  - Antibiotic preparation
  - Biofilm fixation and SEM imaging
  - Wax patterning
  - Fabrication of paper-based transistors
  - Fabrication of paper-based resistors
  - Fabrication of paper-based integrated circuit system
  - Electrical characterization
  - Cross-sectional analysis of transistors
  - Machine learning
- QUANTIFICATION AND STATISTICAL ANALYSIS

SUPPLEMENTAL INFORMATION

Supplemental information can be found online at https://doi.org/10.1016/j.isci.2025.112312.

Received: January 3, 2025
Revised: February 24, 2025
Accepted: March 25, 2025
Published: March 28, 2025

REFERENCES

1. van Belkum, A., Bachmann, T.T., Lüdke, G., Lisby, J.G., Kahlmeter, G., Mohess, A., Becker, K., Hays, J.P., Woodford, N., Mitsakakis, K., et al. (2019). Developmental roadmap for antimicrobial susceptibility testing systems. Nat. Rev. Microbiol. *17*, 51–62. https://doi.org/10.1038/s41579-018-0098-9.
2. Reszetnik, G., Hammond, K., Mahshid, S., AbdElFatah, T., Nguyen, D., Corsini, R., Caya, C., Papenburg, J., Cheng, M.P., and Yansouni, C.P. (2024). Next-generation rapid phenotypic antimicrobial susceptibility testing. Nat. Commun. *15*, 9719. https://doi.org/10.1038/s41467-024-53930-x.
3. Melander, R.J., Zurawski, D.V., and Melander, C. (2018). Narrow-spectrum antibacterial agents. Medchemcomm *9*, 12–21. https://doi.org/10.1039/C7MD00528H.
4. Maxson, T., and Mitchell, D.A. (2016). Targeted Treatment for Bacterial Infections: Prospects for Pathogen-Specific Antibiotics Coupled with Rapid Diagnostics. Tetrahedron *72*, 3609–3624. https://doi.org/10.1016/j.tet.2015.09.069.
5. Kadeřábková, N., Mahmood, A.J.S., and Mavridou, D.A.I. (2024). Antibiotic susceptibility testing using minimum inhibitory concentration (MIC) assays. npj Antimicrob. Resist. *2*, 37. https://doi.org/10.1038/s44259-024-00051-6.
6. Abdul-Aziz, M.H., Alffenaar, J.W.C., Bassetti, M., Bracht, H., Dimopoulos, G., Marriott, D., Neely, M.N., Paiva, J.A., Pea, F., Sjovall, F., et al. (2020). Antimicrobial therapeutic drug monitoring in critically ill adult patients: a Position Paper. Intensive Care Med. *46*, 1127–1153. https://doi.org/10.1007/s00134-020-06050-1.
7. Magréault, S., Jauréguy, F., Carbonnelle, E., and Zahar, J.R. (2022). When and How to Use MIC in Clinical Practice? Antibiotics *11*, 1748. https://doi.org/10.3390/antibiotics11121748.
8. Figueras, A. (2024). A Global Call to Action on Antimicrobial Resistance at the UN General Assembly. Antibiotics *13*, 915. https://doi.org/10.3390/antibiotics13100915.
9. GBD 2021 Antimicrobial Resistance Collaborators (2024). Global burden of bacterial antimicrobial resistance 1990–2021: a systematic analysis with forecasts to 2050. Lancet *404*, 1199–1226. https://doi.org/10.1016/S0140-6736(24)01867-1.
10. Rhee, C., Chen, T., Kadri, S.S., Lawandi, A., Yek, C., Walker, M., Warner, S., Fram, D., Chen, H.C., Shappell, C.N., et al. (2024). Trends in Empiric Broad-Spectrum Antibiotic Use for Suspected Community-Onset Sepsis in US Hospitals. JAMA Netw. Open *7*, e2418923. https://doi.org/10.1001/jamanetworkopen.2024.18923.
11. Oliveira, M., Antunes, W., Mota, S., Madureira-Carvalho, Á., Dinis-Oliveira, R.J., and Dias da Silva, D. (2024). An Overview of the Recent Advances in Antimicrobial Resistance. Microorganisms *12*, 1920. https://doi.org/10.3390/microorganisms12091920.
12. Thornber, K., Bashar, A., Ahmed, M.S., Bell, A., Trew, J., Hasan, M., Hasan, N.A., Alam, M.M., Chaput, D.L., Haque, M.M., and Tyler, C.R. (2022). Antimicrobial Resistance in Aquaculture Environments: Unravelling the Complexity and Connectivity of the Underlying Societal Drivers. Environ. Sci. Technol. *56*, 14891–14903. https://doi.org/10.1021/acs.est.2c00799.
13. Manyi-Loh, C., Mamphweli, S., Meyer, E., and Okoh, A. (2018). Antibiotic Use in Agriculture and Its Consequential Resistance in Environmental Sources: Potential Public Health Implications. Molecules *23*, 795. https://doi.org/10.3390/molecules23040795.
14. Ha, D.R., Haste, N.M., and Gluckstein, D.P. (2019). The Role of Antibiotic Stewardship in Promoting Appropriate Antibiotic Use. Am. J. Lifestyle Med. *13*, 376–383. https://doi.org/10.1177/1559827617700824.
15. Walsh, T.R., Gales, A.C., Laxminarayan, R., and Dodd, P.C. (2023). Antimicrobial Resistance: Addressing a Global Threat to Humanity. PLoS Med. *20*, e1004264. https://doi.org/10.1371/journal.pmed.1004264.
16. Cekin, Z.K., Oncul, A., and Bayraktar, B. (2023). Bloodstream Infections Caused by Multidrug Resistant Bacteria: Clinical and Microbiological Features and Mortality. Sisli Etfal Hastan. Tip Bul. *57*, 416–425. https://doi.org/10.14744/SEMB.2023.31697.
17. Lee, C.R., Cho, I.H., Jeong, B.C., and Lee, S.H. (2013). Strategies to Minimize Antibiotic Resistance. Int. J. Environ. Res. Public Health *10*, 4274–4305. https://doi.org/10.3390/ijerph10094274.
18. Idelevich, E.A., and Becker, K. (2019). How to accelerate antimicrobial susceptibility testing. Clin. Microbiol. Infect. *25*, 1347–1355. https://doi.org/10.1016/j.cmi.2019.04.025.
19. Jacobs, M.R., Colson, J.D., and Rhoads, D.D. (2021). Recent advances in rapid antimicrobial susceptibility testing systems. Expert Rev. Mol. Diagn. *21*, 563–578. https://doi.org/10.1080/14737159.2021.1924679.
20. Gajic, I., Kabic, J., Kekic, D., Jovicevic, M., Milenkovic, M., Mitic Culafic, D., Trudic, A., Ranin, L., and Opavski, N. (2022). Antimicrobial Susceptibility Testing: A Comprehensive Review of Currently Used Methods. Antibiotics *11*, 427. https://doi.org/10.3390/antibiotics11040427.
21. Cella, E., Giovanetti, M., Benedetti, F., Scarpa, F., Johnston, C., Borsetti, A., Ceccarelli, G., Azarian, T., Zella, D., and Ciccozzi, M. (2023). Joining Forces against Antibiotic Resistance: The One Health Solution. Pathogens *12*, 1074. https://doi.org/10.3390/pathogens12091074.
22. Li, Y., Xiao, P., Wang, Y., and Hao, Y. (2020). Mechanisms and control measures of mature biofilm resistance to antimicrobial agents in the clinical context. ACS Omega *5*, 22684–22690. https://doi.org/10.1021/acsomega.0c02294.
23. Sun, F., Qu, F., Ling, Y., Mao, P., Xia, P., Chen, H., and Zhou, D. (2013). Biofilm-associated infections: Antibiotic resistance and novel therapeutic strategies. Future Microbiol. *8*, 877–886. https://doi.org/10.2217/fmb.13.58.
24. Penesyan, A., Paulsen, I.T., Gillings, M.R., Kjelleberg, S., and Manefield, M.J. (2020). Secondary effects of antibiotics on microbial biofilms. Front. Microbiol. *11*, 2109. https://doi.org/10.3389/fmicb.2020.02109.
25. Jamal, M., Ahmad, W., Andleeb, S., Jalil, F., Imran, M., Nawaz, M.A., Hussain, T., Ali, M., Rafiq, M., and Kamil, M.A. (2018). Bacterial biofilm and associated infections. J. Chin. Med. Assoc. *81*, 7–11. https://doi.org/10.1016/j.jcma.2017.07.012.
26. Musken, M., Klimmek, K., Sauer-Heilborn, A., Donnert, M., Sedlacek, L., Suerbaum, S., and Haussler, S. (2017). Towards individualized diagnostics of biofilm-associated infections: a case study. npj Biofilms Microbiomes *3*, 22. https://doi.org/10.1038/s41522-017-0030-5.
27. Kracke, F., Vassilev, I., and Krömer, J.O. (2015). Microbial electron transport and energy conservation – the foundation for optimizing bioelectrochemical systems. Front. Microbiol. *6*, 575. https://doi.org/10.3389/fmicb.2015.00575.
28. Torres, C.I., Marcus, A.K., Lee, H.S., Parameswaran, P., Krajmalnik-Brown, R., and Rittmann, B.E. (2010). A kinetic perspective on extracellular electron transfer by anode-respiring bacteria. FEMS Microbiol. Rev. *34*, 3–17. https://doi.org/10.1111/j.1574-6976.2009.00191.x.
29. Gao, Y., Ryu, J., Liu, L., and Choi, S. (2020). A simple, inexpensive, and rapid method to assess antibiotic effectiveness against exoelectrogenic bacteria. Biosens. Bioelectron. *168*, 112518. https://doi.org/10.1016/j.bios.2020.112518.
30. Rafiee, Z., Rezaie, M., and Choi, S. (2024). Combined Electrical-Electrochemical Phenotypic Profiling of Antibiotic Sustainability of In Vitro Biofilm Models. Analyst *149*, 3224–3235. https://doi.org/10.1039/D4AN00393D.
31. García-Álvarez, L., Busto, J.H., Avenoza, A., Sáenz, Y., Peregrina, J.M., and Oteo, J.A. (2015). Proton Nuclear Magnetic Resonance Spectroscopy as a Technique for Gentamicin Drug Susceptibility Studies with Escherichia coli ATCC 25922. J. Clin. Microbiol. *53*, 2433–2438. https://doi.org/10.1128/jcm.00604-15.
32. Han, J., and Burgess, K. (2010). Fluorescent Indicators for Intracellular pH. Chem. Rev. *110*, 2709–2728. https://doi.org/10.1021/cr900249z.

33. Le Guern, F., Mussard, V., Gaucher, A., Rottman, M., and Prim, D. (2020). Fluorescein Derivatives as Fluorescent Probes for pH Monitoring along Recent Biological Applications. Int. J. Mol. Sci. *21*, 9217. https://doi.org/10.3390/ijms21239217.

34. Xu, X., Chen, S., Yu, Y., Virtanen, P., Wu, J., Hu, Q., Koskiniemi, S., and Zhang, Z. (2022). All-electrical antibiotic susceptibility testing within 30 min using silicon nano transistors. Sens. Actuators B. Chem. *357*, 131458. https://doi.org/10.1016/j.snb.2022.131458.

35. Rivnay, J., Inal, S., Salleo, A., Owens, R.M., Berggren, M., and Malliaras, G.G. (2018). Organic electrochemical transistors. Nat. Rev. Mater. *3*, 17086. https://doi.org/10.1038/natrevmats.2017.86.

36. Pitsalidis, C., Pappa, A.M., Boys, A.J., Fu, Y., Moysidou, C.M., van Niekerk, D., Saez, J., Savva, A., Iandolo, D., and Owens, R.M. (2022). Organic Bioelectronics for In Vitro Systems. Chem. Rev. *122*, 4700–4790. https://doi.org/10.1021/acs.chemrev.1c00539.

37. Shahrim, N.A., Ahmad, Z., Azman, A.W., Buys, Y.F., and Sarifuddin, N. (2021). Mechanisms for doped PEDOT:PSS electrical conductivity improvement. Materi. Adv *2*, 7118–7138. https://doi.org/10.1039/D1MA00290B.

38. Savva, A., Wustoni, S., and Inal, S. (2018). Ionic-to-electronic coupling efficiency in PEDOT:PSS films operated in aqueous electrolytes. J. Mater. Chem. C *6*, 12023–12030. https://doi.org/10.1039/C8TC02195C.

39. Ávila-Niño, J.A., Araujo, E., and González, F. (2023). Study of the doping of PEDOT:PSS films and the reversibility in organic electrochemical transistors. Synth. Met. *299*, 117465. https://doi.org/10.1016/j.synthmet.2023.117465.

40. Niu, Y., Qin, Z., Zhang, Y., Chen, C., Liu, S., and Chen, H. (2023). Expanding the potential of biosensors: a review on organic field effect transistor (OFET) and organic electrochemical transistor (OECT) biosensors. Mater. Futures *2*, 042401. https://doi.org/10.1088/2752-5724/ace3dd.

41. Méhes, G., Roy, A., Strakosas, X., Berggren, M., Stavrinidou, E., and Simon, D.T. (2020). Organic Microbial Electrochemical Transistor Monitoring Extracellular Electron Transfer. Adv. Sci. *7*, 2000641. https://doi.org/10.1002/advs.202000641.

42. Gao, Y., Zhou, Y., Ji, X., Graham, A.J., Dundas, C.M., Miniel Mahfoud, I.E., Tibbett, B.M., Tan, B., Partipilo, G., Dodabalapur, A., et al. (2024). A hybrid transistor with transcriptionally controlled computation and plasticity. Nat. Commun. *15*, 1598. https://doi.org/10.1038/s41467-024-45759-1.

43. Alamer, F.A., Althagafy, K., Alsalmi, O., Aldeih, A., Alotaiby, H., Althebaiti, M., Alghamdi, H., Alotibi, N., Saeedi, A., Zabarmawi, Y., et al. (2022). Review on PEDOT:PSS-Based Conductive Fabric. ACS Omega *7*, 35371035386. https://doi.org/10.1021/acsomega.2c01834.

44. Liu, J., Agarwal, M., and Varahramyan, K. (2008). Glucose sensor based on organic thin film transistor using glucose oxidase and conducting polymer. Sen. Actuators B. Chem. *135*, 195–199. https://doi.org/10.1016/j.snb.2008.08.009.

45. Lingstedt, L.V., Ghittorelli, M., Lu, H., Koutsouras, D.A., Marszalek, T., Torricelli, F., Crăciun, N.I., Gkoupidenis, P., and Blom, P.W.M. (2019). Effect of DMSO Solvent Treatments on the Performance of PEDOT:PSS Based Organic Electrochemical Transistors. Adv. Electron. Mater. *5*, 1800804. https://doi.org/10.1002/aelm.201800804.

46. Hamedi, M.M., Ainla, A., Güder, F., Christodouleas, D.C., Fernández-Abedul, M.T., and Whitesides, G.M. (2016). Integrating Electronics and Microfluidics on Paper. Adv. Mater. *28*, 5054–5063. https://doi.org/10.1002/adma.201505823.

47. Gao, Y., and Choi, S. (2018). Merging Electric Bacteria with Paper. Adv. Mater. Technol. *3*, 1800118. https://doi.org/10.1002/admt.201800118.

48. Tahernia, M., Mohammadifar, M., Gao, Y., Panmanee, W., Hassett, D.J., and Choi, S. (2020). A 96-well high-throughput, rapid-screening platform of extracellular electron transfer in microbial fuel cells. Biosens. Bioelectron. *162*, 112259. https://doi.org/10.1016/j.bios.2020.112259.

49. Gao, Y., Mohammadifar, M., and Choi, S. (2019). From microbial fuel cells to Biobatteries: Moving toward on-demand micro-power generation for Small-scale Single-Use Applications. Adv. Mater. Technol. *4*, 1970039. https://doi.org/10.1002/admt.201900079.

50. Landers, M., Elhadad, A., Rezaie, M., and Choi, S. (2022). Integrated Papertronic Techniques: Highly Customizable Resistor, Supercapacitor, and Transistor Circuitry on a Single Sheet of Paper. ACS Appl. Mater. Interfaces *14*, 45658–45668. https://doi.org/10.1021/acsami.2c13503.

51. Rafiee, Z., Elhadad, A., and Choi, S. (2024). Revolutionizing Papertronics: Advanced Green, Tunable, and Flexible Components and Circuits. Adv. Sustain. Syst. *8*, 2400049. https://doi.org/10.1002/adsu.202400049.

52. Ponce Ortiz, R., Facchetti, A., and Marks, T.J. (2010). High-k Organic, Inorganic, and Hybrid Dielectrics for Low-Voltage Organic Field-Effect Transistors. Chem. Rev. *110*, 205–239. https://doi.org/10.1021/cr9001275.

53. Sau, S., and Kundu, S. (2023). Improved electrical and mechanical properties of highly stretchable polymeric films prepared by blending DMF with the mixed solution of PEDOT:PSS and PVA. Colloids Surf. A: Physicochem. Eng. Asp. *664*, 131082. https://doi.org/10.1016/j.colsurfa.2023.131082.

54. Solazzo, M., Krukiewicz, K., Zhussupbekova, A., Fleischer, K., Biggs, M.J., and Monaghan, M.G. (2019). PEDOT:PSS interfaces stabilised using a PEGylated crosslinker yield improved conductivity and biocompatibility. J. Mater. Chem. B *7*, 4811–4820. https://doi.org/10.1039/C9TB01028A.

55. Thi, M.T.T., Wibowo, D., and Rehm, B.H.A. (2020). Pseudomonas aeruginosa Biofilms. Int. J. Mol. Sci. *21*, 8671. https://doi.org/10.3390/ijms21228671.

56. Rafiee, Z., Rezaie, M., and Choi, S. (2022). Accelerated antibiotic susceptibility testing of Pseudomonas aeruginosa by monitoring extracellular electron transfer on a 3-D paper-based cell culture platform. Biosens. Bioelectron. *216*, 114604. https://doi.org/10.1016/j.bios.2022.114604.

57. Elhadad, A., and Choi, S. (2022). Biofabrication and Characterization of Multispecies Electroactive Biofilms in Stratified Paper-based Scaffolds. Analyst *147*, 4082–4091. https://doi.org/10.1039/D2AN01059C.

58. Spencer, D., Li, Y., Zhu, Y., Sutton, J.M., and Morgan, H. (2023). Electrical Broth Micro-Dilution for Rapid Antibiotic Resistance Testing. ACS Sens. *8*, 1101–1108. https://doi.org/10.1021/acssensors.2c02166.

59. Pang, Z., Raudonis, R., Glick, B.R., Lin, T.J., and Cheng, Z. (2019). Antibiotic resistance in Pseudomonas aeruginosa: mechanisms and alternative therapeutic strategies. Biotechnol. Adv. *37*, 177–192. https://doi.org/10.1016/j.biotechadv.2018.11.013.

60. Poirel, L., Madec, J.Y., Lupo, A., Schink, A.K., Kieffer, N., Nordmann, P., and Schwarz, S. (2018). Antimicrobial Resistance in Escherichia coli. Microbiol. Spectr. *6*, 0026. https://doi.org/10.1128/microbiolspec.arba-0026-2017.

61. Lowy, F.D. (2003). Antimicrobial resistance: the example of Staphylococcus aureus. J. Clin. Investig. *111*, 1265–1273. https://doi.org/10.1172/JCI18535.

STAR★METHODS

KEY RESOURCES TABLE

REAGENT or RESOURCE	SOURCE	IDENTIFIER
Bacterial strains		
Pseudomonas aeruginosa PA01	University of Cincinnati, USA	Daniel J. Hassett
Escherichia coli OP50	Caenorhabditis Genetics Center (CGC)	WBStrain00041969
Staphylococcus aureus subsp. aureus Rosenbach	the American Type Culture Collection (ATCC)	ATCC 6538
Chemicals, peptides, and recombinant proteins		
gentamicin (GEN)	Sigma Aldrich	G4918
ciprofloxacin (CIP)	Sigma Aldrich	17850
ceftazidime (CEF)	Sigma Aldrich	A6987
glutaraldehyde	Sigma Aldrich	G7776
phosphate-buffered saline	Sigma Aldrich	806544
PEDOT:PSS	Heraeus	Clevios PH1000
3-glycidoxypropyltrimethoxysilane	Sigma Aldrich	440167
dimethyl sulfoxide	Avantor®	97061-250
polyvinyl alcohol	Avantor®	10118-164
Graphene powder	Sigma Aldrich	900561
Software and algorithms		
MATLAB (version 2017b)	Mathworks	https://www.mathworks.com/
Origin	OriginLab	https://www.originlab.com/
Other		
Whatman™ 3MM chromatography paper	Avantor®	21427-364

EXPERIMENTAL MODEL AND STUDY PARTICIPANT DETAILS

This work did not need any unique experimental model.

METHOD DETAILS

Bacterial inoculum

The bacterial strains Pseudomonas aeruginosa, Escherichia coli, and Staphylococcus aureus were cultivated in Luria Broth (LB) medium, adjusted to a pH of 7.0. The LB formulation included 10 g/L tryptone, 5 g/L sodium chloride, and 5 g/L yeast extract, dissolved in 1 liter of DI water. Cultures were incubated at 37°C for about 6 hours until reaching an optical density at 600 nm (OD600) of 1.0, equivalent to approximately 10^9 CFU/mL. Following incubation, the cultures were centrifuged at 4000 rpm for 4 minutes to pellet the bacterial cells. The supernatant was carefully removed, and the cell pellets were resuspended in fresh LB medium. Resuspension was achieved through vigorous mixing with a vortex to ensure homogeneous distribution of cells in the medium. To prevent contamination during the multi-hour test, all samples were handled in a sterile biosafety cabinet and covered with sterilized plastic caps throughout incubation.

Antibiotic preparation

Three antibiotics, each representing a distinct family, were chosen as model compounds: gentamicin (GEN) from the aminoglycosides, ciprofloxacin (CIP) from the fluoroquinolones, and ceftazidime (CEF) from the cephalosporins. GEN disrupts protein synthesis and compromises the integrity of bacterial outer membranes. CIP inhibits DNA replication, effectively halting bacterial growth, while CEF, a third-generation cephalosporin, impedes bacterial cell wall synthesis. To determine the MICs for each pathogen, dilution series were prepared in sterile LB medium. All experiments were conducted using LB medium for consistency across species and antibiotic conditions. The concentrations ranged as follows: GEN (0, 2, 4, 8, 16, and 32 μg/mL), CIP (0, 0.25, 0.5, 1, 1.5, and 2 μg/mL), and CEF (0, 2, 4, 8, 16, and 32 μg/mL).

Biofilm fixation and SEM imaging

Biofilm-forming bacterial cells were immobilized onto engineered cellulose fibers using 2.5% glutaraldehyde in 0.1 M phosphate-buffered saline (PBS), incubating the samples overnight for fixation. Following fixation, the samples underwent dehydration through a graded ethanol series, with sequential exposure to 35%, 50%, 75%, 95%, and 100% ethanol. Once dehydrated, the samples were left in a desiccator to dry overnight. The dried samples were then coated with a thin layer of carbon using a 208HR Turbo Sputter Coater (Cressington Scientific Instruments, UK). For imaging and analysis, a field emission scanning electron microscope (FE-SEM, Supra 55 VP, Carl Zeiss AG, Germany) was employed.

Wax patterning

To fabricate all paper-based electronic components, including integrated circuits, we utilized Whatman^{TM} 3MM chromatography paper with dimensions of 20 cm × 20 cm, a thickness of 340 μm, and a flow rate of 130 mm/30 min, sourced from VWR International. Wax pattern designs were created using AutoCAD software and printed using a Xerox ColorQube 8570 wax printer, which was calibrated to match the paper size. For double-sided printing, careful alignment was ensured to maintain precision on both sides. After printing, the wax was thermally diffused into the paper by heating it at 150°C. By adjusting the heating duration, we controlled the penetration depth of the wax and the volume of the hydrophilic regions, allowing us to fine-tune the paper's functional properties.

Fabrication of paper-based transistors

The vertical field-effect transistor was fabricated using a configuration based on our previous work. In this design, the gate electrode was positioned on the bottom surface of the paper substrate, while the source and drain electrodes were accessible from the top. Following the wax patterning step to delineate the transistor region, the fabrication process commenced with the incorporation of a gate dielectric layer into the paper substrate. The dielectric material was prepared by dissolving 1 g of PVA in 10 mL of DI water at 90°C. Precise control over heating time and temperature was essential to achieve optimal viscosity and controlled diffusion within the paper matrix. The channel region was subsequently infused with a p-type semiconductor ink formulated from 1 wt% PEDOT:PSS (Clevios PH1000, Heraeus) mixed with 5 wt% DMSO to enhance conductivity. To further improve hydrophilicity, a 2 wt% solution of 3-glycidoxypropyltrimethoxysilane (3-GLYMO) was introduced, optimizing the channel's performance and compatibility with aqueous environments. This engineered channel region provided a tunable conductive interface, offering ionic conductivity while serving as a hydrophilic and porous reservoir for bacterial cultures. After assembling the transistor structure, the device was air-dried overnight under ambient conditions to ensure uniform material integration into the paper substrate. Once the structure was stabilized, electrodes were deposited. The gate electrode was applied to the bottom surface, while the source and drain electrodes were deposited on the top. A conductive ink comprising PEDOT:PSS blended with 5 wt% graphene powder was used for all electrodes, ensuring enhanced electrical conductivity and stability. The ink was dispensed using a precision inkjet printing technique, allowing for accurate and reproducible electrode deposition. This fabrication approach resulted in a robust, functional transistor structure, with integrated features tailored to support bacterial culture and real-time sensing in paper-based platforms.

Fabrication of paper-based resistors

The resistors were engineered with a vertically oriented circular configuration, incorporating rectangular extensions at both ends to facilitate electrical connectivity. These extensions were specifically designed for seamless integration with PCBs. A single-sided wax printing technique was employed to fabricate the extensions, enabling precise definition of their geometry and ensuring consistent and reliable electrical interfacing with PCB components. The resistive ink was prepared by blending 50% PEDOT:PSS with DI water, optimized to achieve the desired resistance values and informed by methodologies established in previous studies.

Fabrication of paper-based integrated circuit system

A complete circuit system was constructed on a single sheet of paper, incorporating resistors to enable effective operation of the p-type transistor for AST applications. The terminals of the circuit components were interconnected using conductive traces printed on both sides of the paper. These traces were created via direct inkjet printing, using a composite ink made from PEDOT:PSS mixed with 5 wt% graphene powder. This approach ensured robust electrical connectivity and seamless integration within the paper-based platform.

Electrical characterization

The conductance and resistance of the resistors and conductive traces were measured using a Lomvum T28B multimeter and a four-point probe setup. The paper transistor's transfer and output characteristics were analyzed with the Keithley 4200-SCS semiconductor characterization system. Voltage measurements were performed using a DataQ acquisition system to ensure precise and reliable data collection.

Cross-sectional analysis of transistors

To obtain a clean cross-section for analysis, the transistors underwent a controlled freezing process using liquid nitrogen, followed by fracturing at their midpoint. The resulting cross-sections were examined using a Hitachi SU5000 Field Emission Scanning Electron Microscope (FE-SEM) and a V12 Stereo Optical Microscope, enabling detailed structural characterization.

Machine learning

The system captures voltage-vs.-time signals from the AST sensor, which are first subjected to noise filtering and baseline correction. The algorithm then compares each processed signal against reference profiles for GEN, CIP, and CEF, computing an MSE that identifies the closest antibiotic match and classifies it as 'below MIC,' 'at MIC,' or 'above MIC.' By leveraging these reference profiles, we can rapidly and accurately determine the antibiotic's potency relative to the bacteria being tested. Figures 5 and S4 present the data used for algorithm training and validation, while Figure 6 illustrates the overall classification accuracy and highlights the efficacy of this method in real-time AST analyses. During blind testing, the antibiotic identity/concentration was withheld from the algorithm. Each sample was tested multiple times, and the MSE classifier predicted both the antibiotic and whether it was above, at, or below the MIC threshold. We observed that ~25–100 repeat tests yielded consistent success rates.

QUANTIFICATION AND STATISTICAL ANALYSIS

The experimental results presented in this study were obtained from a minimum of three independent replicates. Data are expressed as the mean ± standard error, ensuring reliability and consistency in interpretation. Beyond this, no specific statistical analysis or quantification was conducted in this study.